


Article

Microstructure and Wear Property of Graphene Nanoplatelets Reinforced Nickel-Based Composite Coating by Laser Cladding

Bin Han, Ge Li, Zubin Chen *  and Guoguang Zhang

School of Materials Science and Engineering, China University of Petroleum (East China), Qingdao 266580, China; hbzjh@upc.edu.cn (B.H.); lige1014qingdao@163.com (G.L.); zhangggupc@163.com (G.Z.)

* Correspondence: czbcu@163.com

Abstract: Nickel-based composite coatings containing graphene nanoplatelets (GNPs) were prepared on Q235 steel using laser cladding. In order to retain the multilayer GNPs in the composite coatings after laser cladding, NiGNPs were prepared by electroless nickel plating on GNPs as the additive phase. All the coatings contain γ -(Ni, Fe), Cr_{23}C_6 , Cr_7C_3 , Fe_3C and WC phases, and multilayer GNPs were retained successfully in the composite coatings. With the addition of GNPs, the microstructure of the coatings was obviously refined and the content of Cr-C compounds were increased along with its changed morphology. The mean microhardness of the Ni-based composite coatings containing GNPs was significantly improved compared to that of Ni45 coating, and the maximum microhardness was 745.06 when 20% NiGNPs was added. The results indicated that, due to the refinement and lubricating effects of GNPs, the friction coefficients of composite coatings were reduced and the wear resistance was improved compared to Ni45 coating.

Keywords: Ni-based composite coatings; GNPs; laser cladding; wear resistance



Citation: Han, B.; Li, G.; Chen, Z.; Zhang, G. Microstructure and Wear Property of Graphene Nanoplatelets Reinforced Nickel-Based Composite Coating by Laser Cladding. *Metals* **2022**, *12*, 1247. <https://doi.org/10.3390/met12081247>

Academic Editors: Célia de Fraga Malfatti and Claudia Beatriz Dos Santos

Received: 15 June 2022

Accepted: 23 July 2022

Published: 25 July 2022

Publisher's Note: MDPI stays neutral with regard to jurisdictional claims in published maps and institutional affiliations.



Copyright: © 2022 by the authors. Licensee MDPI, Basel, Switzerland. This article is an open access article distributed under the terms and conditions of the Creative Commons Attribution (CC BY) license (<https://creativecommons.org/licenses/by/4.0/>).

1. Introduction

Surface modification by coating is an effective way to improve the surface properties of the metal substrate and prolong the service life of the workpiece [1,2]. Recently, surface modification technologies for alloys have mostly been performed by laser sintering [3], electrochemical deposition [4], thermal spraying [2], surfacing welding [5] and laser cladding [6]. Among these, laser cladding is most widely used to obtain high-quality metallurgical bonding coatings owing to its simplicity, high processing efficiency and accuracy, automation control, concentrated energy with a small heat-affected zone and low damage to the substrate [7].

Nickel-based alloy coatings are widely used in marine, chemical, nuclear industry and machinery fields owing to their toughness, strong oxidation resistance and high corrosion resistance [8]. Given the rapid development of industrialization and the complicated operating environment, it is important that the wear resistance of the coatings, especially for the service life of minerals machinery, is developed further. The issues can be solved by preparing the nickel-based composite coating by adding various reinforcing phases into the alloy. At present, B_4C , TiC, WC and Cr_3C_2 are used as reinforcing phases for nickel-based alloys [9,10]. However, these carbide-reinforcing phases have a tendency to produce stress concentration, with cracks and holes therefore forming in the cladding layer [11]. Graphene, a type of carbon nanomaterial, has been widely used as a reinforcing phase owing to its unique two-dimensional structure and excellent mechanical properties, which can avoid the disadvantages of the above reinforcing phases [12,13]. Meanwhile, graphene possesses a special single-atom layer structure and many excellent thermal and mechanical properties: 130 GPa of the strength, $\sim 5000 \text{ J}/(\text{m}\cdot\text{K}\cdot\text{s})$ of thermal conductivity and excellent self-lubricating properties. These excellent properties of graphene have prompted it to be one of the most desirable reinforcing phases.

In this work, graphene nanoplatelets (GNPs) were electroless nickel plated to solve the problem of GNPs ablation during laser cladding, and then the plated GNPs were added into nickel-based powders as the reinforcement phase; meanwhile, laser cladding technology was used to prepare nickel-based composite coatings with high hardness, wear resistance, friction reduction and corrosion resistance on the key friction pairs surfaces. The microstructure evolution of nickel-based composite coatings with different GNPs contents were analyzed. Then, the hardness, friction coefficient and wear resistance of nickel-based composite coatings containing different GNPs contents were also presented.

2. Experimental Procedures

Due to its low cost, high strength, strong plasticity and good welding performance, Q235 steel is widely used in industry [14]. In this work, the chemical composition of Q235 steel with the dimension of 90 mm × 70 mm × 10 mm listed in Table 1 was used as the substrate for laser cladding. Before laser cladding, the rust, grease and other impurities on the substrate surface were removed. The self-made SD-Ni45 powder was used as the based powder, and the chemical composition was shown in Table 2. SD-Ni45 powder is spherical, with a diameter of 48–100 μm. Graphene nanoplatelets (GNPs, thickness: 4–20 nm, layers: <30) were used as the additive phase, and the microstructure characterization was illustrated in Figure 1.

Table 1. Chemical composition of Q235 steel (wt. %).

Elements	C	Mn	Si	S	P	Fe
Contents	≤0.22	0.3~0.65	≤0.35	≤0.05	≤0.045	Bal.

Table 2. Chemical composition of SD-Ni45 powder (wt. %).

Elements	C	Cr	Mn	Si	B	WC	Fe	Ni
Contents	0.55	14	0.13	2.5	1.9	20	14.2	Bal.

The original structure of graphene makes it likely to be destroyed during laser cladding. This problem was effectively solved by electroless nickel plating on the surface of the GNPs. This is a bright spot and an improvement of the current processes, which has important significance and application value. The nickel-plated graphene nanoplatelets (NiGNPs) were obtained, and the content of GNPs in NiGNPs was about 1.3–1.7% (wt. %). The microstructure characterization of NiGNPs is shown in Figure 1. The Raman results indicated that the characteristic peaks of D, G and 2D appeared in the GNPs sample ($I_G/I_D = 8.40$) was not observed in NiGNPs, while a nickel diffraction peak existed. The bulk samples were used for XRD and the results also showed that the C(002) and C(004) diffraction peaks of GNPs completely disappeared after electroless nickel plating, while Ni diffraction peaks appeared. These results indicated that the GNPs surface was successfully covered with a metallic nickel coating layer after nickel plating. In this work, the content of 10%, 20% and 30% NiGNPs were selected to be added to SD-Ni45 powder, respectively, to prepare composite coatings using a Torch Light 6000W fiber laser equipment with wavelength of 980 nm, manufactured by Shandong Energy Heavy Equipment Manufacturing Co., Ltd., Taian, China. The rectangular light spot with the size of 18 mm × 2 mm was used for laser cladding. Eight passes of laser cladding overlap tests were carried out on each plate. In the early stage, the effects of laser cladding power of 1000–4000 W and scanning speed of 100–600 mm/min on microstructure and properties of coatings were investigated. The results showed that the coating hardness decreases due to the high laser energy density when the power is too high or the scanning rate is too slow, while the coating forming is poor if the power is too low or the scanning speed is too fast. Based on process parameter optimization, the related cladding parameters were listed in Table 3, and no shielding gas was used during cladding. Pre-laid powder was used in this work, and the schematic diagram of laser cladding was shown in our previous work [15].

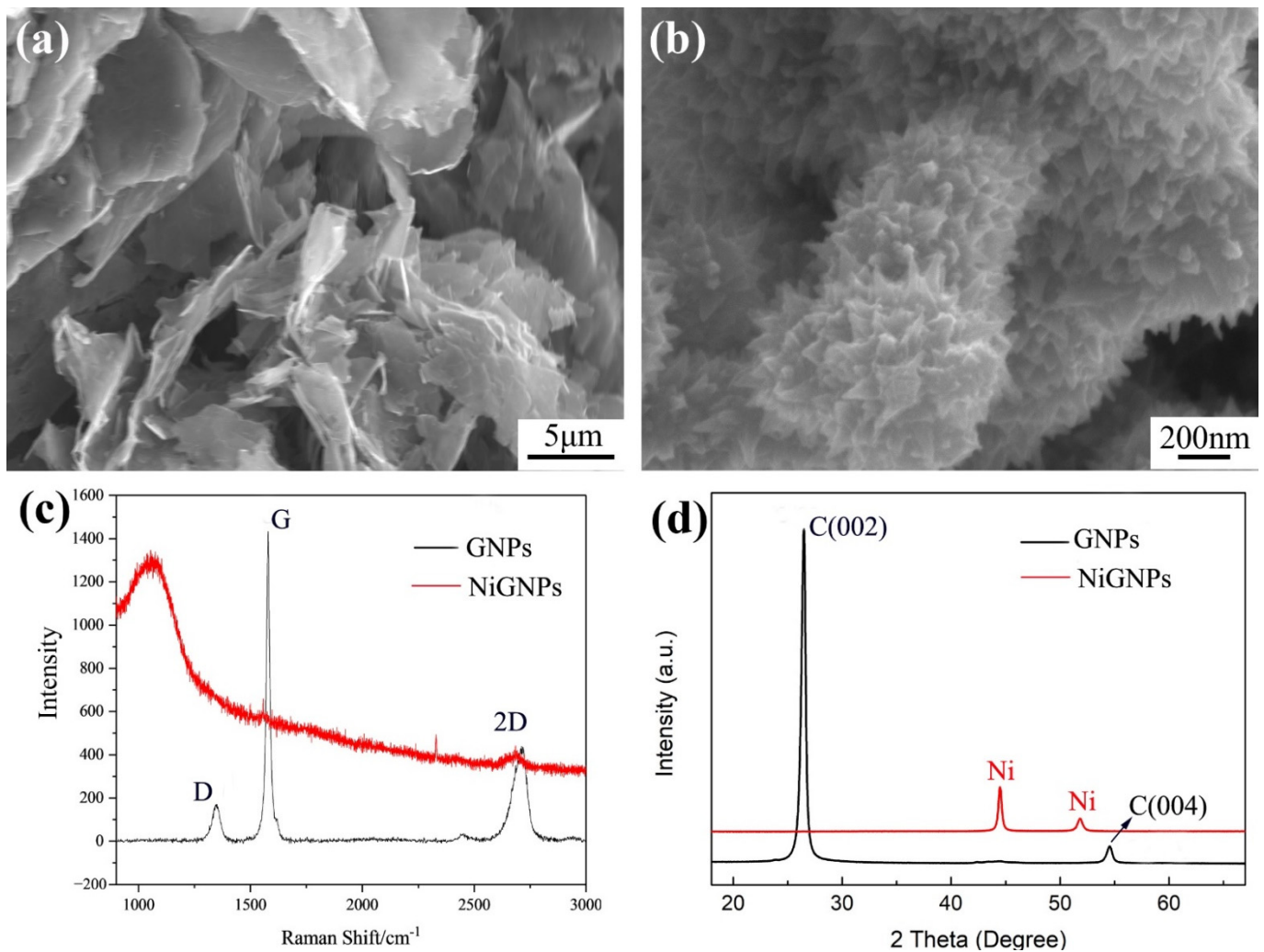


Figure 1. Microstructure analyses of GNPs and NiGNPs: (a) SEM image of GNPs, (b) SEM image of NiGNPs, (c) Raman patterns, (d) XRD patterns.

Table 3. Laser cladding parameters of GNPs reinforced nickel-based composite coatings.

Laser Power (W)	Scanning Speed (mm/min)	Powder Thickness (mm)	Overlapping Rate (%)
3000	480	1	30

The surface morphology and microstructure of GNPs reinforced nickel-based composite coatings were characterized by scanning electron microscope (SEM, JSM-7200F, JEOL, Tokyo, Japan) equipped with energy-dispersive spectroscopy (EDS, OXFORDX-MAX50, UK). The phase composition of the cladding layer was analyzed by X-ray diffractometer (XRD, X'PERT PRO MPO, Panaco Inc., Netherlands). The microhardness of coatings was measured by a microhardness tester (HV-1000, Beijing Times ChuangHe Technology Co., Ltd., Beijing, China). The loading load was 100 g and the holding time was 15 s. The first point of each sample was measured 10 μm away from the coating surface and then a hardness point was measured every 10 μm from the start point to the end of the matrix. The hardness test was repeated three times and then the average value was taken. WTM-2E controlled atmosphere micro friction and a wear tester was used to measure the wear properties of composite coatings with the wear time of 30 min at room temperature. The grinding ball with diameter of 3 mm was GCr15 bearing steel, the normal load was 800 g, the motor speed was 500 r/min, and the radius of rotation was 3 mm. The hardness of the GCr15 ball was 65HRC. The sample size of friction and wear test was 15 mm \times 15 mm \times 10 mm.

Before the test, SiC sandpaper of grit 180#, 320#, 600# and 1000# were used to grind the surface, and SEM results showed that the tested surface was the middle microstructure of the coatings. The weight of the specimen before and after the wear test was recorded.

3. Results and Discussion

3.1. Microstructure

Figure 2 showed the XRD patterns of four composite coatings with different GNPs contents. All four coatings contain γ -(Ni, Fe), Cr_{23}C_6 , Cr_7C_3 , Fe_3C and WC phases. Compared with the Ni45 coating, the composite coatings containing GNPs have additional diffraction peaks at about 26.5° and 54.5° , which is related to the characteristic peak of C(002) and C(004) of multilayer graphene [16,17]. With the increase of GNPs content, the characteristic peaks of graphene become more obvious. This indicated that GNPs can be successfully retained in the nickel-based composite coatings after laser cladding. Notably, the diffraction peaks of grains along (111) and (200) crystal planes were enhanced with the addition of GNPs, indicating that GNPs could promote grain growth on (111) and (200) planes. Meanwhile, the peak strength of diffraction peaks of Cr_{23}C_6 , Cr_7C_3 and other carbides increased as the increasing of GNPs content. During laser cladding, GNPs can react with strong carbide elements such as Cr to form Cr-rich carbides, thus, the Cr-rich carbides content in the nickel-based composite coating increases.

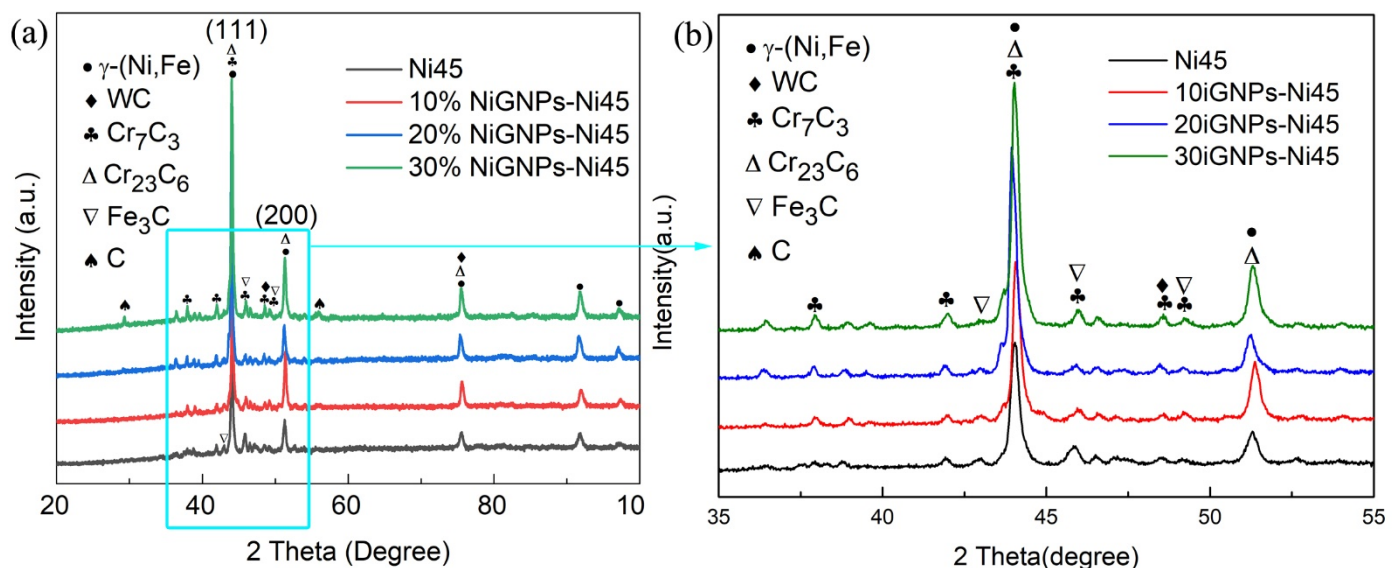


Figure 2. XRD patterns of different content of graphene nanosheets reinforced nickel-based composite coatings. (a) full patterns (b) Magnified patterns between 35° and 55° .

Figure 3 showed the surface microstructure of nickel-based composite coatings with different GNPs contents. It can be seen that the Ni45 coating was mainly composed of the square block (Spot A), triangle-like shape (Spot B), rod-like (Spot C), irregular shape (Spot D) and thin strip network (Spot E). From the EDS results shown in Table 4 combined with XRD patterns above, Spots A, B and C were mainly composed of Cr and C elements, which are related to Cr_7C_3 and Cr_{23}C_6 , respectively. Spot D was γ -(Ni, Fe) solid solution due to the main composition of Fe and Ni elements, while Spot E was a carbides eutectic microstructure composed of Cr, Fe and Ni elements. With the addition of GNPs, the morphology and quantity of Cr-rich carbides in the coatings were changed. In the cladding layer, the precipitates of Cr-rich carbides with large bar-like and sheet-like morphology were formed. The eutectic microstructure also changed gradually from a thin strip network to a granular network and the area of Cr-carbide in the composite coatings increased. Some research indicated [18] that graphene can improve the nucleation rate and promote

crystallization, thus, the grains could be refined, resulting in the refinement of eutectic microstructure in the cladding layer.

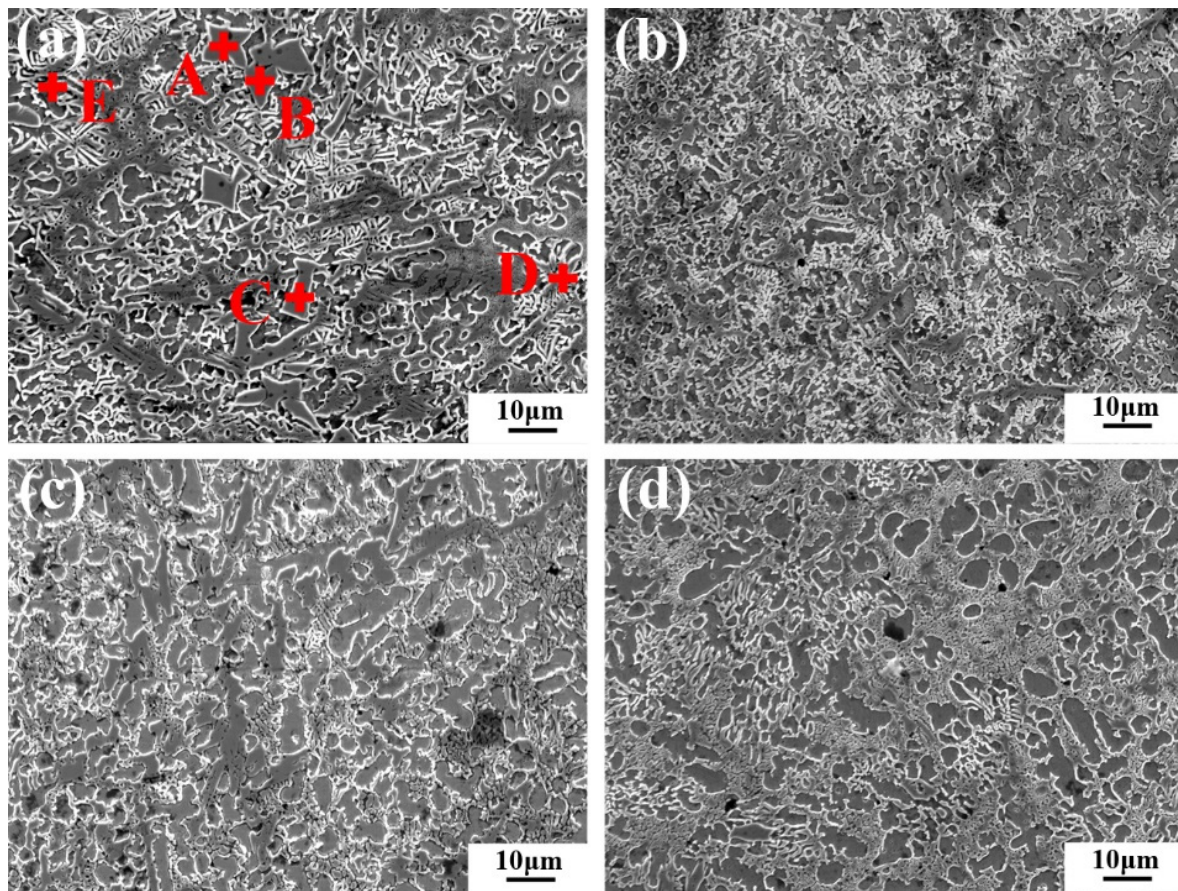


Figure 3. SEM images of surface microstructure of Ni-based composite coatings with different NiGNPs content: (a) 0, (b) 10%, (c) 20%, (d) 30%.

Table 4. EDS results of each point shown in Figure 3 (at %).

Spot	Fe	Ni	C	Cr	W	Possible Phase
A	12.8	9.8	18.7	53.3	5.4	Cr ₇ C ₃
B	12.3	9.0	15.9	56.6	6.2	Cr ₂₃ C ₆
C	16.9	9.5	14.8	54.3	4.5	Cr ₂₃ C ₆
D	21.2	53.5	18.3	6.1	0.8	γ-(Ni, Fe)
E	19.6	18.6	26.0	32.0	3.8	Cr-Fe-Ni-C

Figures 4 and 5 showed the SEM images of the cross-sectional microstructure of Ni-based composite coatings with different GNPs content. Figure 4 showed the overall cross-sectional nickel-based composite coatings, which revealed that a sound metallurgical bonding between the cladding layer and the substrate was achieved with different GNPs content added, i.e., a high adhesion existed between the coating and the substrate. The final thickness of the coatings decreased with the increase of the added GNPs content, and the coating thickness is 816 µm, 798 µm, 785 µm and 768 µm for the NiGNPs content of 0, 10%, 20% and 30%, respectively. Ni45 coating was briefly shown in Figure 5(a1–a3). In the bottom part of the coating, the flat crystal grew near the interface between the cladding layer and substrate due to the small supercooling degree, and then the columnar crystal grew perpendicular to the flat crystal along the direction of heat flow in the solidification process. In the middle part, the microstructure gradually turned into dendrites. In the upper part, equiaxed grains or cellular grains were gradually formed due to the large supercooling

degree. The EDS results of Spot A and B shown in Figure 5(a1) were 45.3 Fe-17.4 Ni-25.8 C-10.4 Cr-0.9 W and 50.9 Fe-20.8 Ni-23.2 C-4.6 Cr-0.5 W, respectively. The content of the C element and Cr element at Spot A in the interdendritic zone is significantly higher than that at Spot B (dendritic zone). As GNPs were added, the cross-sectional microstructure of the nickel-based composite coatings from the bottom to the upper was shown in Figure 5b–d. From the bottom to upper part of the coatings, the flat crystal and columnar crystal (perpendicular to the flat crystal), dendrites (central cladding layer) and the cellular crystal (upper part of cladding layer) were presented, while the growth of the columnar crystal was not as severe as that in Ni45 coating. This indicates that GNPs do not change the microstructure morphology of the coatings significantly; however, they can inhibit the growth of columnar crystals. Meanwhile, the microstructure of composite coatings was refined as GNPs were added. It could be seen that some porosity existed in the coating when the addition of NiGNPs content reached 20%, as shown in Figure 4. As GNPs content increased, the melt viscosity and the tendency of GNPs agglomeration during the laser cladding process was increased [19]. Some research assumes these porosities to be bubbles porosities. The driving force of the formation of gas porosities is usually linked to the formation of CO or CO₂ gas which originated from oxidation processes, and which are then entrapped within the melt while failing to diffuse out, depending on the processing parameters [20,21]. Thus, the porosities were easily generated.

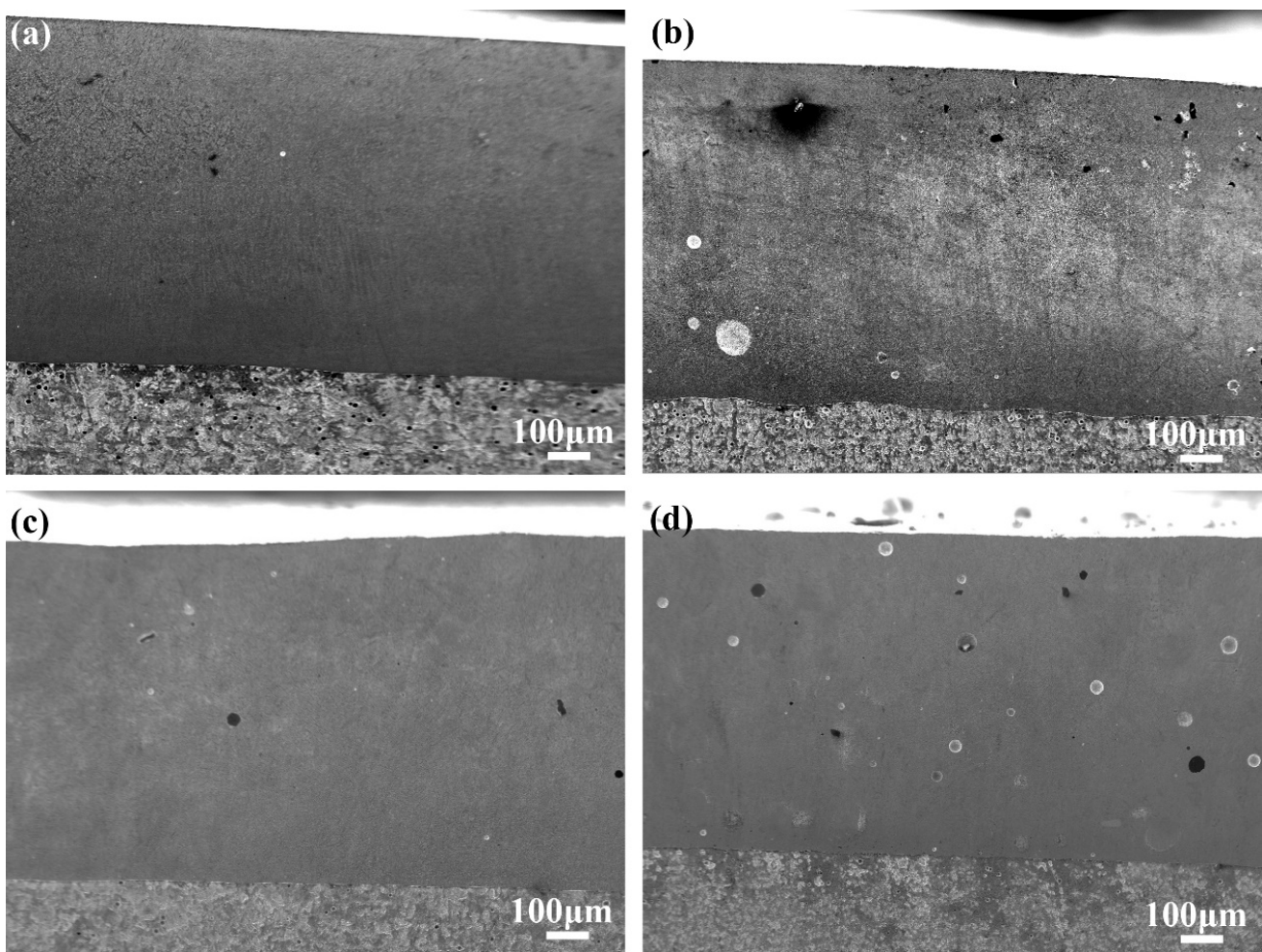


Figure 4. SEM images of overall cross-sectional nickel-based composite coatings with different NiGNPs content: (a) 0, (b) 10%, (c) 20% and (d) 30%.

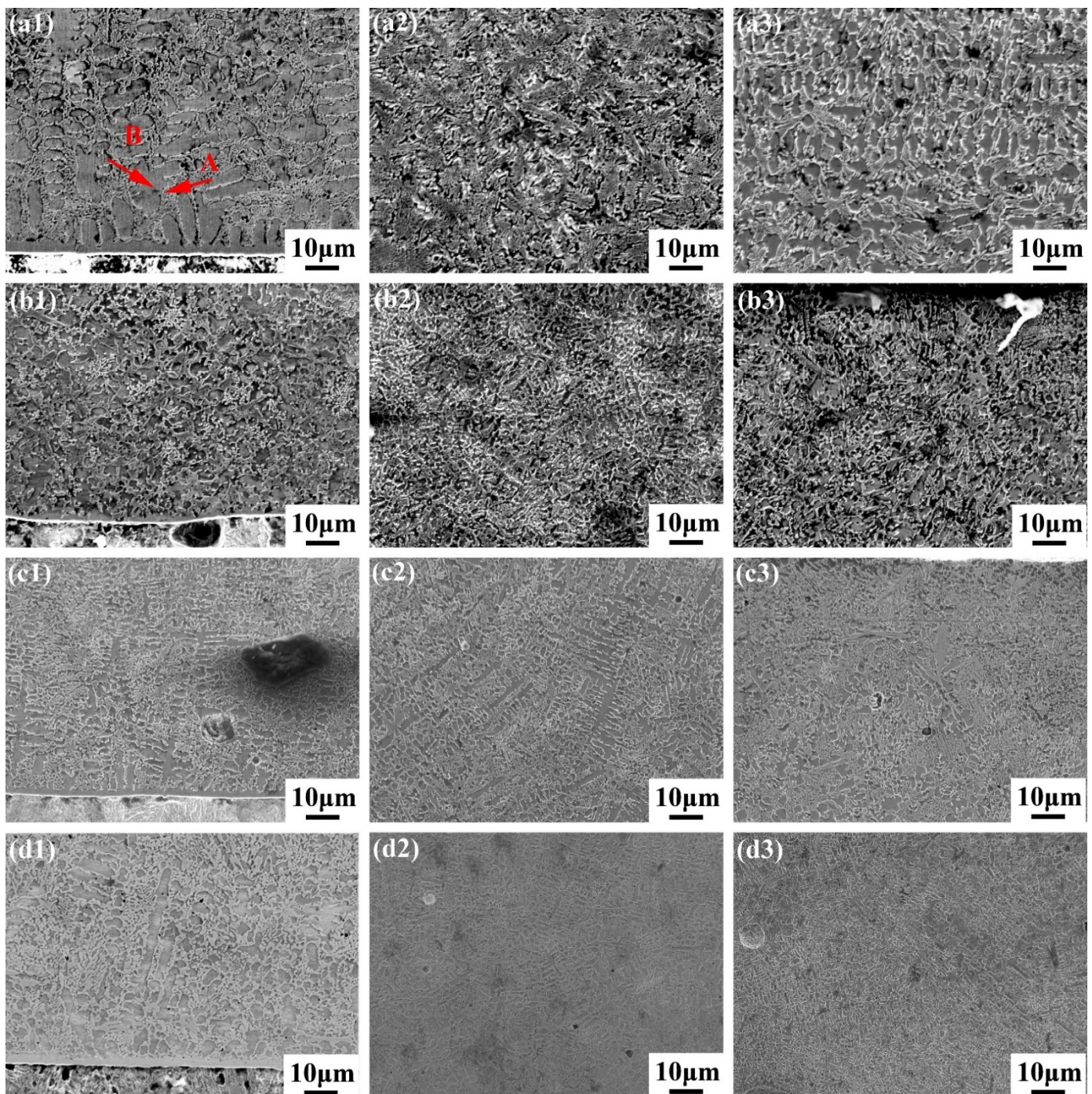


Figure 5. SEM images of cross-sectional nickel-based composite coatings with different NiGNPs content: (a) 0, (b) 10%, (c) 20% and (d) 30%. Numbers 1, 2 and 3 represent the bottom, middle and upper microstructure of the corresponding coating, respectively.

The characteristic peak of GNPs in different composite coatings was detected by XRD shown in Figure 2, which indicated that graphene existed in the composite coatings prepared by laser cladding. Raman analyses were used to further confirm the existence of GNPs in the composite coating, and the results were shown in Figure 6. It was seen that D, G and 2D peaks of graphene existed, which indicated that graphene does exist in the laser-cladding nickel-based composite coatings [22]. Meanwhile, the ratios of area G and area D peaks of GNPs in the nickel-based composite coatings added with 10%, 20% and 30% NiGNPs after laser cladding (I_G/I_D) were calculated as 1.07, 1.03 and 1.05,

respectively. The G peaks are associated with ideal graphitic carbons, whereas the D peaks are related to the structural defects of C-C bond [23]. Usually, the ratio of I_G/I_D is used to characterize the damage degree of GNPs [24]. The decreased value of I_G/I_D after laser cladding indicated that the laser beam with high energy density caused the damage of GNPs structure, resulting in the increased density of structural defects of GNPs [25]. The intensity of 2D peak of GNPs in the Ni-based composite coatings with the addition of 30% was lower than that in the low addition composite coatings, and the ratio of G peak and 2D peak (I_G/I_{2D}) of GNPs in the composite coatings added with 10%, 20% and 30% NiGNPs were calculated as 1.34, 1.32 and 1.41, respectively. The I_G/I_{2D} presents the number of graphene layers, indicating the agglomeration intensity of graphene under the same conditions [26]. Therefore, as the addition of NiGNPs was 30%, the GNPs were agglomerated seriously, which lead to the occurrence of blowhole in the composite coating during the laser cladding process.

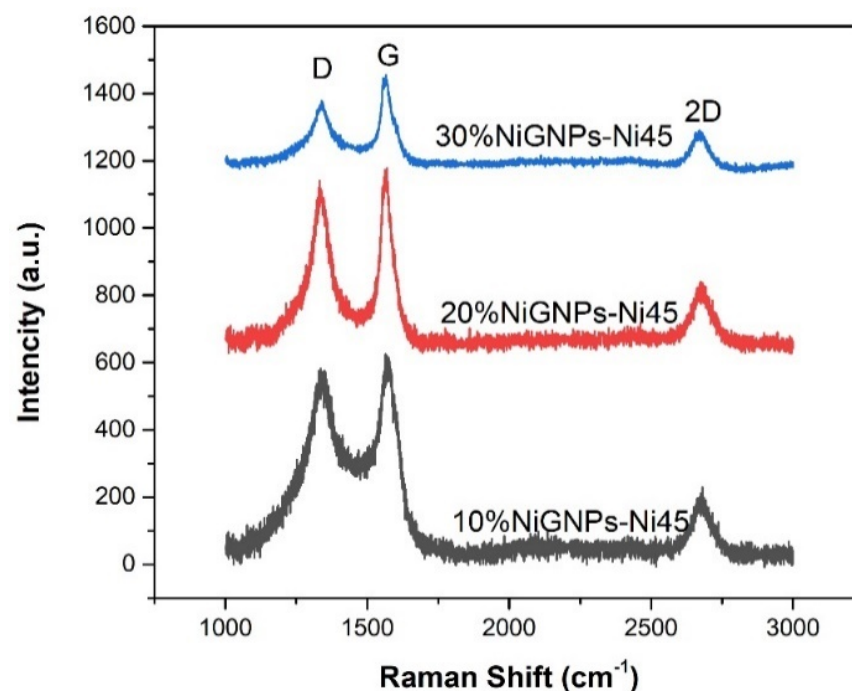


Figure 6. Raman analyses of GNPs in nickel-based graphene composite coating.

3.2. Mechanical Properties

3.2.1. Microhardness

Figure 7 showed the mean microhardness and cross-sectional microhardness distribution of Ni-based composite coatings with different GNPs content. The mean microhardness of Ni-based coatings with different GNPs content were 555.58, 659.09, 745.06 and 671.78, respectively. The mean microhardness of three Ni-based composite coatings containing GNPs was significantly improved compared to that of the Ni45 coating. With the increase of GNPs content, the microhardness of the Ni-based composite coatings was gradually increased first and then decreased. The increased microhardness of the Ni-based composite coating may be attributed to the facts listed as follows. Firstly, the thermal conductivity of GNPs is much higher than that of the substrate, and the large supercooling degree could be generated due to the difference between GNPs and substrate during laser cladding, which lead to the refinement of microstructure [27]. The above analysis of the microstructure (Figures 3 and 5) has verified this; the refined microstructure of the coating possessed the increased microhardness with the increase of GNPs content. Similarly, the microstructure of different coating parts is slightly different, resulting in the microhardness curve of coating parts being slightly fluctuated. In addition, the improvement could be attributed to GNPs-strengthening phases constraining the local deformation of the composite coatings

during the indentation [28]. Finally, the increased microhardness of the coatings may be related to the increased amount of carbides due to the melt and reaction of GNPs [29]. It was noted that the microhardness of the coating was decreased when the NiGNPs content exceeded 20%, which resulted from the aggregation phenomenon of GNPs in the un-dense cladding layer. The similar results can be seen in Ref. [30] and the aggregation phenomenon of GNPs was verified Figures 9 and 10 in this work. Moreover, the heterogeneous size and distribution of grains in the 30% NiGNPs-Ni45 composite coating decreased the uniformity of the microhardness.

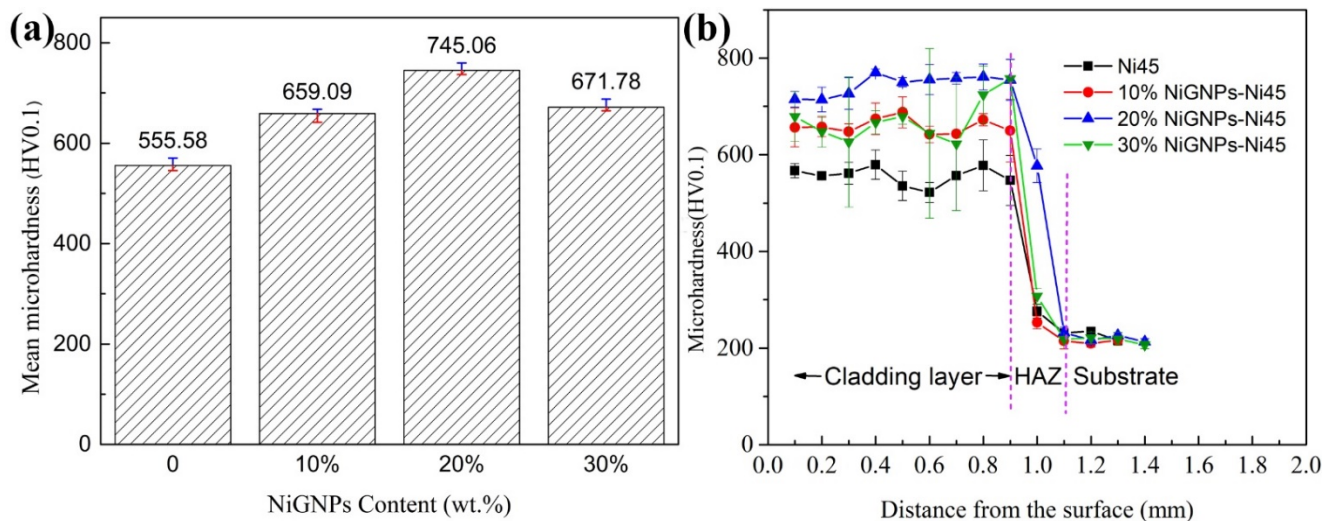


Figure 7. (a) Mean microhardness and (b) cross-sectional microhardness distribution of Ni-based composite coatings with different GNPs content.

3.2.2. Friction and Wear Property

Friction coefficient is one of the effective methods of evaluating the wear resistance of coatings, and the low friction coefficient often means a better friction reduction effect. Figure 8 showed the friction coefficient curves and loss weight histograms of Ni-based composite coatings with different GNPs content. It can be seen that different trends of friction coefficient curves were obtained for different coatings. For Ni45 coating, except for the initial wear stage, the friction coefficient possessed a platform stable stage. When GNPs were added, the friction coefficient of the coatings decreased successively after reaching the maximum value. The final friction coefficient of the three coatings added-GNPs was significantly decreased compared to Ni45 coating [31], and the friction coefficient of the composite coatings decreased first and then increased with the increase of GNPs content from Figure 8a. The final friction coefficient of 20% NiGNPs-Ni45 cladding layer obtained the lowest value of 0.388, which is lower than the friction coefficient of 0.47 of laser cladding coating when 10% TiC, TiN and B4C are added to the powder Ni204 [32]. The friction coefficient of composite coatings with the addition of 10% or 20% NiGNPs had a higher value in the early wear period ($3 \text{ s} < t \leq 900 \text{ s}$) than in the later wear period; however, the friction coefficients of both composite coatings during all wear periods were lower than that of Ni45 coating. After 900s, the friction coefficients of the two nickel-based composite coatings containing NiGNPs (10% and 20%) decreased gradually, and finally stabilized around 0.385–0.401. During the early wear period, the fine microstructure and hard carbides in 10% NiGNPs-Ni45 and the 20% NiGNPs-Ni45 cladding layer were worn, making the friction coefficients of two composite coatings lower than that of the Ni45 sample. As the wear progressed, GNPs embedded in the composite coatings were ground. GNPs is a two-dimensional material with a special structure, where a weak van der Waals force between layers are existed, giving GNPs a self-lubricating property. Therefore, the wear of the cladding layer was lowered and the friction coefficients of composite coatings were gradually decreased [33]. It is noted that the friction coefficient of the 30% NiGNPs-

Ni45 cladding layer increased again compared to that of the other two composite coatings, probably due to the relatively large content of GNPs in the 30% NiGNPs-Ni45 sample. The agglomeration of GNPs reduced the compactness of the microstructure of the 30% NiGNPs-Ni45 cladding layer during laser cladding. The enhancement effect of GNPs on cladding layer was therefore weakened, resulting in the slight reduce of friction coefficient of the coating.

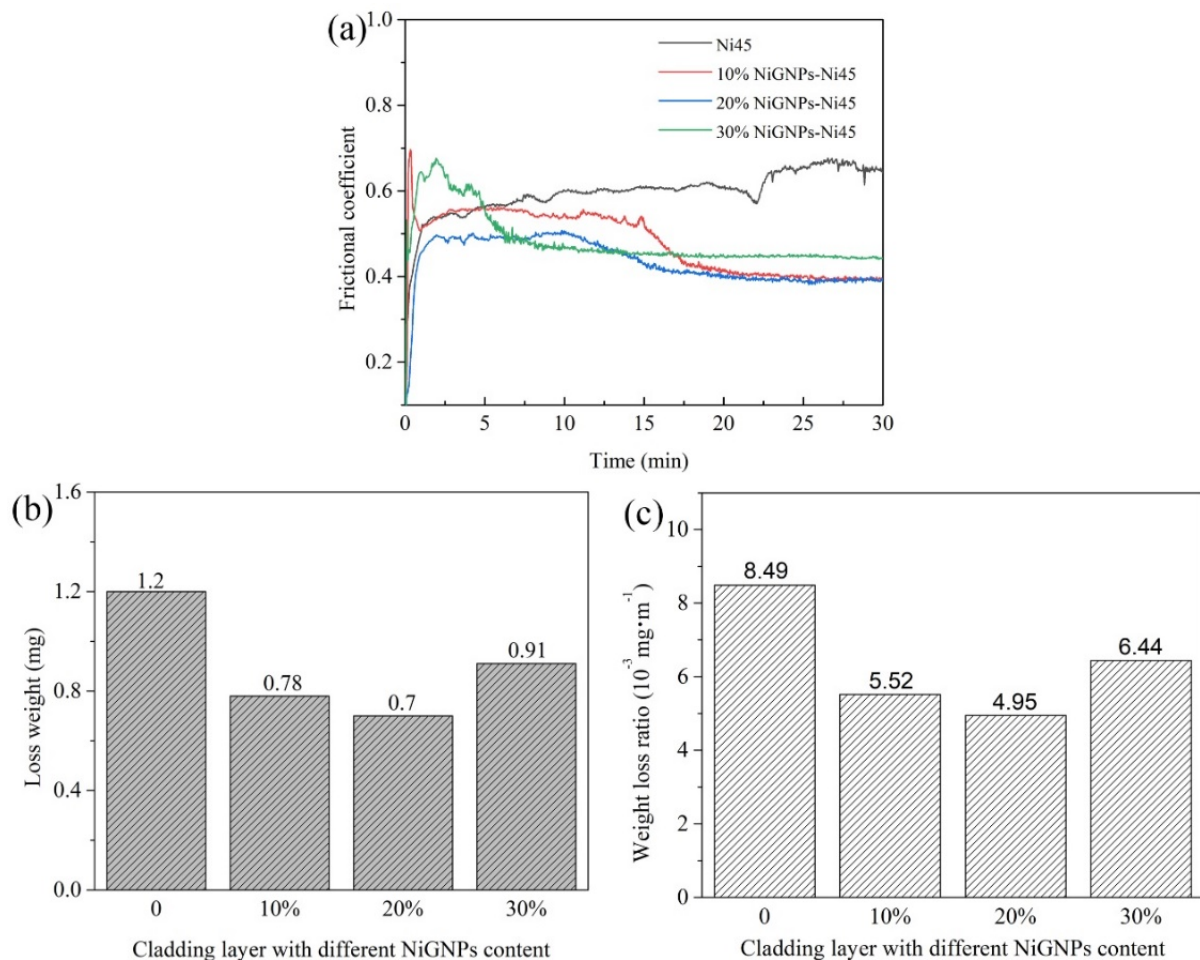


Figure 8. (a) Friction coefficient curves, (b) histogram of loss weight and (c) histogram of weight loss ratio of Ni-based cladding layer with different NiGNPs content.

Loss weight and loss weight ratio are the indexes to evaluate the wear resistance of materials. The loss weight ratio (w) is calculated as follows:

$$w = \frac{m}{\pi \cdot d \cdot n} \quad (1)$$

where m is the loss weight of the sample, d is the diameter of the grinding ball and n represents the total number of turns of the grinding. Figure 8b,c showed the comparison of loss weight and loss weight ratio of four nickel-based coatings with different GNPs content. It can be seen that the Ni45 coating had the highest loss weight with the value of 1.2 mg, while the 20% NiGNPs-Ni45 sample possess the lowest value of 0.7 mg. The loss weight ratio of four nickel-based coatings with different GNPs content were calculated as 8.49×10^{-3} mg/m, 5.52×10^{-3} mg/m, 4.95×10^{-3} mg/m and 6.44×10^{-3} mg/m, respectively. Obviously, with the increase of GNPs content, the wear resistance of the Ni-based composite coatings was first gradually increased and then decreased, and the highest wear resistance was achieved when 20% NiGNPs was added, which was consistent with the results and analyses of the friction coefficient of the four coatings.

Figure 9 showed the worn morphology of the four nickel-based coatings with different GNPs content, and the corresponding EDS results were shown in Table 5. The width of the wear tracks was increased as the addition of GNPs, and the average value was 294.7 μm , 350.5 μm , 422.1 μm and 628.4 μm for Ni45 coating, 10% NiGNPs-Ni45, 20% NiGNPs-Ni45 and 30% NiGNPs-Ni45 coating, respectively. As seen in Figure 9a–b, large numbers of fine, granular and floc debris with large areas of flake shedding (micro-holes) existed at the worn surface of Ni45 coating, and furrows parallel to the wear direction were observed. From Figure 9c–h, with the addition of GNPs, the wear debris on the worn surface of the coating was significantly reduced compared to that of Ni45 sample. Meanwhile, the furring phenomenon was not obvious, with a relatively reduced degree of flake shedding. This indicated that the wear resistance of the coating containing GNPs was higher than that of the Ni45 coating. From the EDS results shown in Table 5, the flocking and granular debris were mainly composed of Fe, Ni, Cr and C elements. During the wear process, the hard phases fall off when the grinding ball is constantly rubbed, forming peeling pits and furrows in the wear track and producing wear debris on the surface. The furrow was the typical characteristic of abrasive wear and debris was the typical characteristic of adhesive wear, while microstructure spalling was the main feature of fatigue wear [34]. Thus, the mixed mechanisms of abrasive and fatigue wear occurred on the worn surface of coatings.

It is noted that some C-rich phase was observed on the worn surface of composite coatings, which may be retained GNPs due to the analyses above. Raman analyses were performed at the worn surface of the nickel-base composite coatings with different GNPs content to further verify the C-rich phase, and the results were shown in Figure 10. It was seen that D, G and 2D peaks existed, which were typical characteristic peaks of GNPs. Therefore, the C-enriched phases existed at the worn surface of composite coatings were GNPs. As can be seen from Figure 10, the GNPs showed different morphology, with a multilayer structure characterized by wrinkles and folds at the worn surface of the nickel-based composite coatings, which is quite different from the original GNPs morphology shown in Figure 1a. GNPs patch could be spread along the sliding direction due to the role of cyclic stress, which is characterized by the laminated sheets with different sizes shown in Figure 10a,c,e. Compared with the low GNPs content (10% and 20%) composite coatings, micro-holes existed at the worn surface of 30% NiGNPs-Ni45 sample, which was also observed shown in Figure 4d. The wear debris was relatively increased, with small flakes of microstructure spalling. This indicated that the wear resistance of 30% NiGNPs-Ni45 sample was slightly lower than that of the other two composite coatings, which was also consistent with the friction coefficient results shown in Figure 8.

In general, the reasons for the excellent wear resistance and friction reduction of the Ni-based composite coatings containing GNPs could be summarized as follows. Firstly, GNPs refine the grain size and improves the hardness of the coatings. Generally speaking, the higher the hardness, the better the wear resistance. Secondly, GNPs, a two-dimensional material with special structure, has a weak van der Waals force between the layers, which makes it possess good self-lubrication performance; the contact surface enriched GNPs can provide a lubricating effect [35].

Through this work, some prospects for coating research can be suggested. In the coating study, it is necessary to further study the volume fraction of each phase and use the BSE model to characterize the phases' natures and morphologies. During the laser cladding process, shielding gas should be used, which can influence porosities occurrence within the clad coatings. In the analysis of wear mechanism, coating microstructure, porosity and the actual nature of the debris, especially oxides, should be taken into account. This could be the subject of one or more other works to be published later.

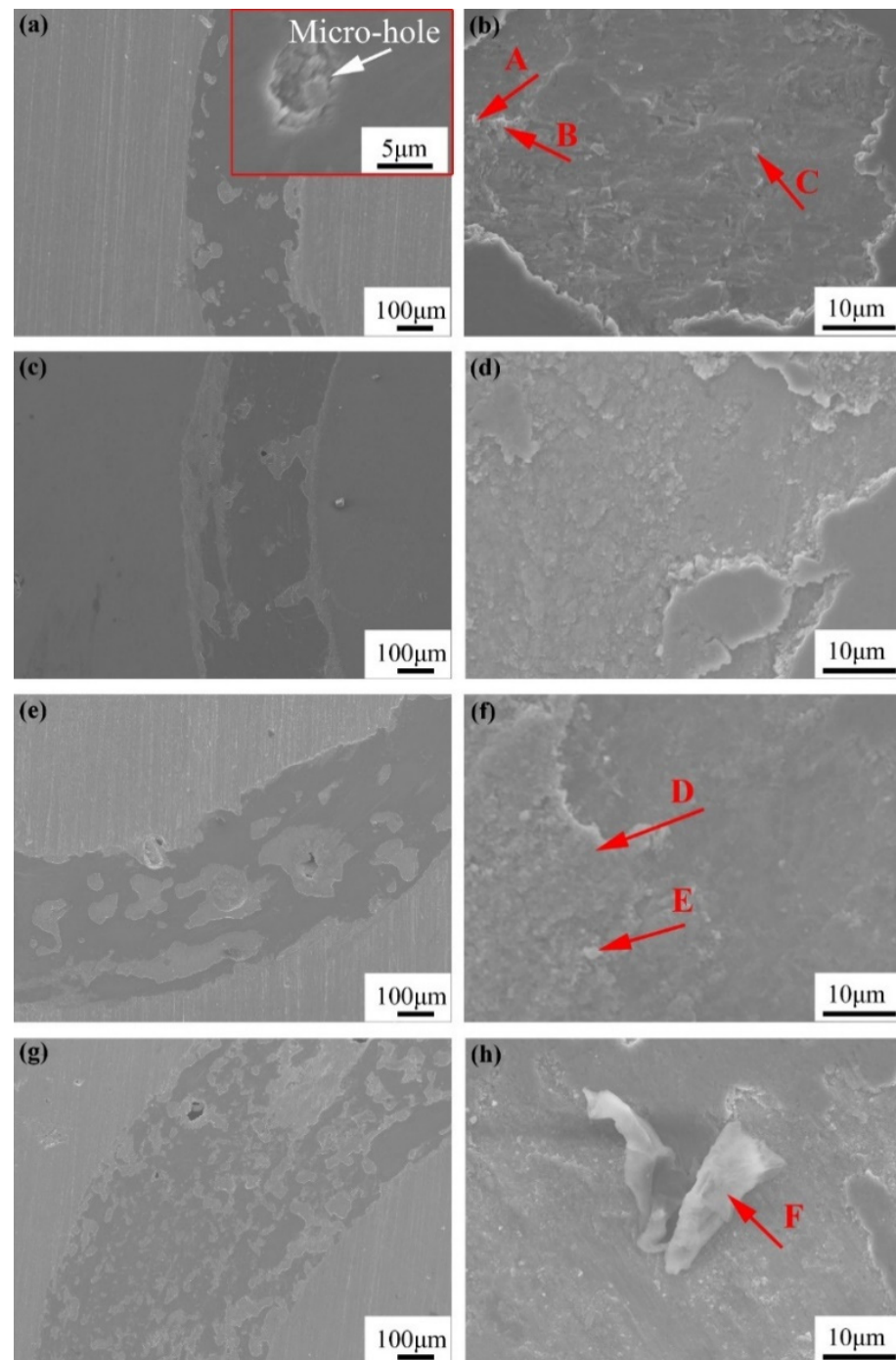


Figure 9. Worn morphology of nickel-based composite coatings with different NiGNPs content: (a,b) 0, (c,d) 10% 0, (e,f) 20% 0, (g,h) 30%.

Table 5. EDS results of each spot shown in Figure 9 (at %).

Spot	Fe	Ni	C	Cr	W
A	49.6	10.7	33.0	5.5	0.7
B	49.8	4.9	42.4	2.3	0.4
C	36.0	29.3	22.2	11.2	1.3
D	72.1	2.6	23.2	1.5	0.6
E	67.6	2.3	28.3	1.6	0.5
F	22.0	0.8	76.5	0.5	0.1

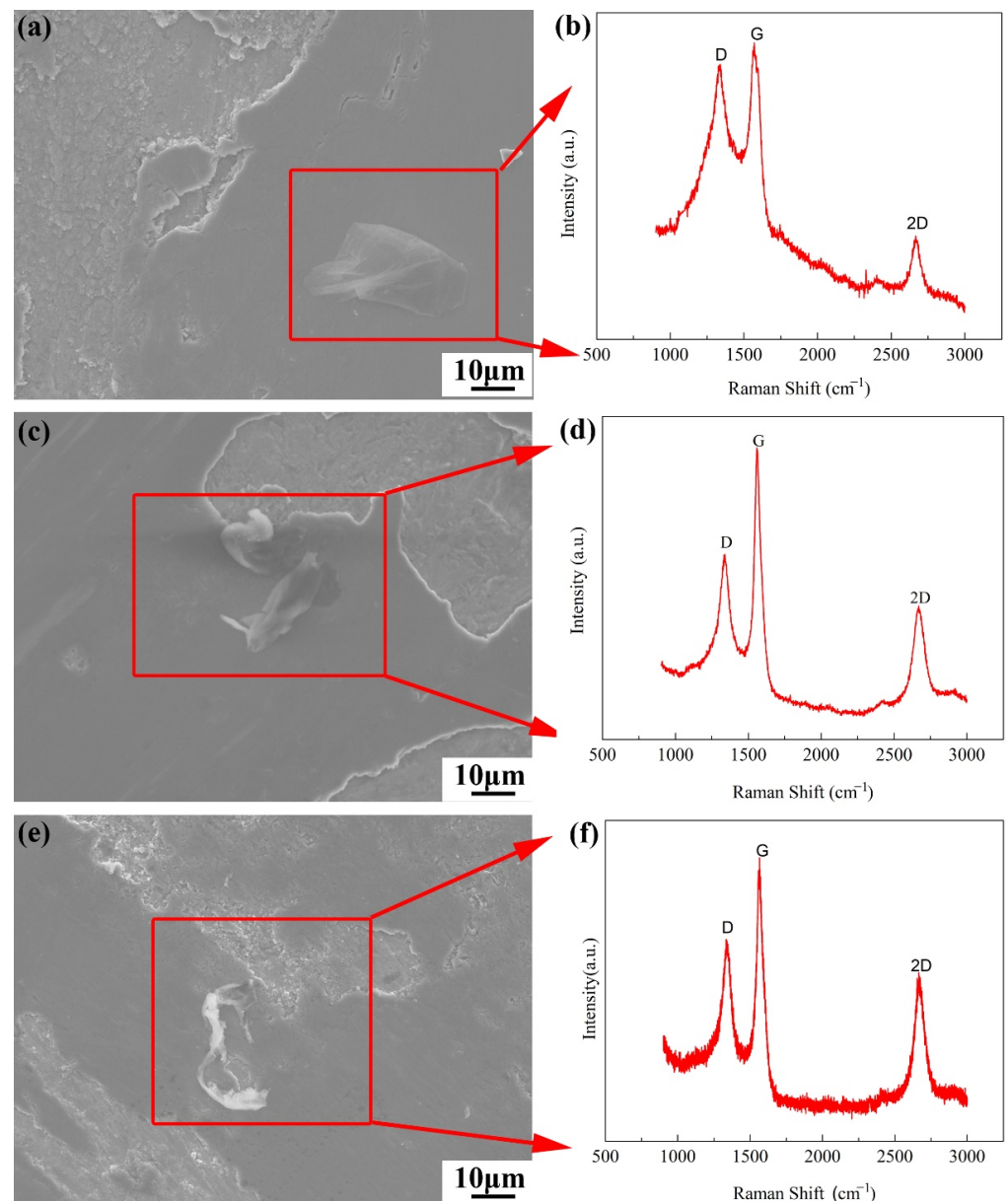


Figure 10. SEM images and corresponding Raman results of GNPs in nickel-based composite coatings with different NiGNPs content: (a,b) 10%, (c,d) 20%, (e,f) 30%.

4. Conclusions

Nickel-based composite coatings containing different GNPs content were successfully prepared on Q235 steel by laser cladding technology. The microstructure and wear property of the four nickel-based coatings were studied in detail. The main conclusions were listed as follows:

- (1) All the four coatings contain γ -(Ni, Fe), Cr_{23}C_6 , Cr_7C_3 , Fe_3C and WC phases. Besides, multilayer GNPs were retained successfully in the nickel-based composite coatings when GNPs were added.
- (2) With the addition of GNPs, the growth of columnar crystals of the coatings were inhibited and the microstructure of the composite coatings were obviously refined. Meanwhile, the content of Cr-C compounds increased and its morphology was changed, and the eutectic structure was gradually changed into granular network. When the GNPs content reached 30%, the serious agglomeration of GNPs led to gas porosi-

ties appearing in the composite coating during the laser cladding process, and the compactness of the cladding layer was reduced.

- (3) The mean microhardness of the Ni-based composite coatings containing GNPs was significantly improved compared to that of the Ni45 coating. With the increase of GNPs content, the microhardness of the Ni-based composite coatings was increased first and then decreased, and the maximum mean microhardness of Ni-based composite coating was 745.06 when 20% NiGNPs was added.
- (4) With the addition of GNPs, the friction coefficient was reduced and the wear resistance was improved compared to the Ni45 coating, which was due to the refinement effect and lubricating effect of GNPs.

Author Contributions: Conceptualization, G.L. and G.Z.; methodology, G.L.; validation, G.L., B.H. and G.Z.; formal analysis, G.L.; investigation, G.L.; resources, G.L.; data curation, G.L.; writing—original draft preparation, Z.C.; writing—review and editing, Z.C.; visualization, G.L.; supervision, B.H. and Z.C.; project administration, B.H.; funding acquisition, B.H. and Z.C. All authors have read and agreed to the published version of the manuscript.

Funding: This research was funded by the National Natural Science Foundation of China, grant number 51771228, the Fundamental Research Funds for the Central Universities, China, grant number 21CX06051A, and the Major Science and Technology Projects of PetroChina, grant number ZD2019-184-004.

Institutional Review Board Statement: Not applicable.

Informed Consent Statement: Not applicable.

Data Availability Statement: The raw/processed data required to reproduce these findings cannot be shared at this time as the data also forms part of an ongoing study.

Conflicts of Interest: The authors declare no conflict of interest.

References

1. Humam, S.B.; Gyawali, G.; Amanov, A.; Kim, T.H.; Lee, S.W. Microstructure, interface, and nanostructured surface modifications to improve mechanical and tribological performance of electrodeposited Ni-W-TaC composite coating. *Surf. Coat. Technol.* **2021**, *419*, 127293. [\[CrossRef\]](#)
2. Amanov, A.; Karimbaev, R.; Berkebile, S.P. Effect of ultrasonic nanocrystal surface modification on wear mechanisms of thermally-sprayed WC-Co coating. *Wear* **2021**, *477*, 203873. [\[CrossRef\]](#)
3. Jing, W.; Hui, C.; Qiong, W.; Hongbo, L.; Zhanjun, L. Surface modification of carbon fibers and the selective laser sintering of modified carbon fiber/nylon 12 composite powder. *Mater. Des.* **2017**, *116*, 253–260. [\[CrossRef\]](#)
4. Truc, N.T.; Minh, H.H.; Khanh, L.L.; Thuy, V.M.; Van Toi, V.; Van Man, T.; Nam, H.C.N.; Quyen, T.N.; Hiep, N.T. Modification of type I collagen on TiO₂ surface using electrochemical deposition. *Surf. Coat. Technol.* **2018**, *344*, 664–672. [\[CrossRef\]](#)
5. Peddiraju, V.C.; Pulapakura, K.K.; Jagadeesh, D.S.; Athira, K.; Gudur, S.; Suryakumar, S.; Chatterjee, S. Weld deposition of nickel on titanium for surface hardening with Ti-Ni-based intermetallic compounds. *Mater. Today Proc.* **2020**, *27*, 2096–2100. [\[CrossRef\]](#)
6. Kim, C.K.; Choi, S.G.; Kim, J.H.; Jo, H.J.; Jo, Y.-C.; Choi, S.-P.; Cho, Y.T. Characterization of surface modification by laser cladding using low melting point metal. *J. Ind. Eng. Chem.* **2020**, *87*, 54–59. [\[CrossRef\]](#)
7. Liu, X.; Bi, J.; Meng, Z.; Li, R.; Li, Y.; Zhang, T. Tribological behaviors of high-hardness Co-based amorphous coatings fabricated by laser cladding. *Tribol. Int.* **2021**, *162*, 107142. [\[CrossRef\]](#)
8. Adesina, O.; Oki, M.; Farotade, G.; Ogunbiyi, O.; Adeleke, A. Effect of nickel-based laser coatings on phase composition and corrosion behaviour of titanium alloy for offshore application. *Mater. Today Proc.* **2021**, *38*, 830–834. [\[CrossRef\]](#)
9. Zhao, Y.; Yu, T.; Sun, J.; Jiang, S. Microstructure and properties of laser clad B₄C/TiC/Ni-based composite coating. *Int. J. Refract. Met. Hard Mater.* **2020**, *86*, 105112. [\[CrossRef\]](#)
10. Zhang, D.; Zhang, X. Laser cladding of stainless steel with Ni-Cr₃C₂ and Ni-WC for improving erosive-corrosive wear performance. *Surf. Coat. Technol.* **2005**, *190*, 212–217. [\[CrossRef\]](#)
11. Xiao, Q.; Sun, W.L.; Yang, K.X.; Xing, X.F.; Chen, Z.H.; Zhou, H.N.; Lu, J. Wear mechanisms and micro-evaluation on WC particles investigation of WC-Fe composite coatings fabricated by laser cladding. *Surf. Coat. Technol.* **2021**, *420*, 127341. [\[CrossRef\]](#)
12. Deng, P.; Yao, C.; Feng, K.; Huang, X.; Li, Z.; Li, Y.; Zhao, H. Enhanced wear resistance of laser clad graphene nanoplatelets reinforced Inconel 625 superalloy composite coating. *Surf. Coat. Technol.* **2018**, *335*, 334–344. [\[CrossRef\]](#)
13. Zhao, Z.; Bai, P.; Misra, R.; Dong, M.; Guan, R.; Li, Y.; Zhang, J.; Tan, L.; Gao, J.; Ding, T.; et al. AlSi10Mg alloy nanocomposites reinforced with aluminum-coated graphene: Selective laser melting, interfacial microstructure and property analysis. *J. Alloys Compd.* **2019**, *792*, 203–214. [\[CrossRef\]](#)

14. Huang, L.; Wang, S.-S.; Li, H.-J.; Wang, J.-Y.; Li, Z.-G.; Wu, Y.-C. Highly effective Q235 steel corrosion inhibition in 1 M HCl solution by novel green strictosamide from *Uncaria laevigata*: Experimental and theoretical approaches. *J. Environ. Chem. Eng.* **2022**, *10*, 107581. [[CrossRef](#)]
15. Zhang, S.; Han, B.; Li, M.; Zhang, Q.; Hu, C.; Jia, C.; Li, Y.; Wang, Y. Microstructure and high temperature erosion behavior of laser cladded CoCrFeNiSi high entropy alloy coating. *Surf. Coat. Technol.* **2021**, *417*, 127218. [[CrossRef](#)]
16. Sadoun, A.M.; Abdallah, A.W.; Najjar, I.M.R.; Basha, M.; Elmahdy, M. Effect of lattice structure evolution and stacking fault energy on the properties of Cu–ZrO₂/GNP nanocomposites. *Ceram. Int.* **2021**, *47*, 29598–29606. [[CrossRef](#)]
17. Zia, F.; Zia, K.M.; Aftab, W.; Tabasum, S.; Nazli, Z.-I.; Mohammadi, M.; Zuber, M. Synthesis and characterization of graphene nanoplatelets-hydroxyethyl cellulose copolymer-based polyurethane bionanocomposite system. *Int. J. Biol. Macromol.* **2020**, *165*, 1889–1899. [[CrossRef](#)]
18. Patil, A.; Nartu, M.S.K.K.Y.; Ozdemir, F.; Banerjee, R.; Gupta, R.K.; Borkar, T. Enhancement of the mechanical properties of graphene nanoplatelet (GNP) reinforced nickel matrix nanocomposites. *Mater. Sci. Eng. A* **2021**, *817*, 141324. [[CrossRef](#)]
19. Hassanzadeh-Aghdam, M.K.; Ansari, R.; Deylami, H.M. Influence of graphene nano-platelets on thermal transport performance of carbon fiber-polymer hybrid composites: Overall assessment of microstructural aspects. *Int. J. Therm. Sci.* **2022**, *171*, 107209. [[CrossRef](#)]
20. Liu, Z.; Kim, H.; Liu, W.; Cong, W.; Jiang, Q.; Zhang, H. Influence of energy density on macro/micro structures and mechanical properties of as-deposited Inconel 718 parts fabricated by laser engineered net shaping. *J. Manuf. Process.* **2019**, *42*, 96–105. [[CrossRef](#)]
21. Zhan, X.; Qi, C.; Gao, Z.; Tian, D.; Wang, Z. The influence of heat input on microstructure and porosity during laser cladding of Invar alloy. *Opt. Laser Technol.* **2019**, *113*, 453–461. [[CrossRef](#)]
22. Da, K.; Xu, L.; Lei, L.; Hu, W.; Wu, Y. Graphene–nickel composites. *Appl. Surf. Sci.* **2013**, *273*, 484–490.
23. Qin, J.; Zhu, S.; Feng, C.; Zhao, N.; Shi, C.; Liu, E.-Z.; He, F.; Ma, L.; Li, J.; He, C. In-situ space-confined catalysis for fabricating 3D mesoporous graphene and their capacitive properties. *Appl. Surf. Sci.* **2018**, *433*, 568–574. [[CrossRef](#)]
24. Johannes, L.B.; Yowell, L.L.; Sosa, E.; Arepalli, S.; Mishra, R.S. Survivability of single-walled carbon nanotubes during friction stir processing. *Nanotechnology* **2006**, *17*, 3081–3084. [[CrossRef](#)]
25. Chen, Y.; Lu, F.; Zhang, K.; Nie, P.; Hosseini, S.R.E.; Feng, K.; Li, Z. Laser powder deposition of carbon nanotube reinforced nickel-based superalloy Inconel 718. *Carbon* **2016**, *107*, 361–370. [[CrossRef](#)]
26. Sharma, A.; Sharma, V.M.; Paul, J. A comparative study on microstructural evolution and surface properties of graphene/CNT reinforced Al6061–SiC hybrid surface composite fabricated via friction stir processing. *Trans. Nonferrous Met. Soc. China* **2019**, *29*, 2005–2026. [[CrossRef](#)]
27. Xu, J.; Lin, X.; Guo, P.; Dong, H.; Wen, X.; Li, Q.; Xue, L.; Huang, W. The initiation and propagation mechanism of the overlapping zone cracking during laser solid forming of IN-738LC superalloy. *J. Alloys Compd.* **2018**, *749*, 859–870. [[CrossRef](#)]
28. Turan, M.E.; Sun, Y.; Akgul, Y.; Turen, Y.; Ahlatci, H. The effect of GNPs on wear and corrosion behaviors of pure magnesium. *J. Alloys Compd.* **2017**, *724*, 14–23. [[CrossRef](#)]
29. Jiang, H.; Zhu, Y.; Butt, D.P.; Alexandrov, I.V.; Lowe, T.C. Microstructural evolution, microhardness and thermal stability of HPT-processed Cu. *Mater. Sci. Eng. A* **2000**, *290*, 128–138. [[CrossRef](#)]
30. Ezatpour, H.; Parizi, M.T.; Ebrahimi, G.; Gupta, M.; Li, J.; Guo, W. Effect of hybrid carbonaceous reinforcement on structure, mechanical and wear properties of spark plasma sintered CrCoFeMnNi HEA/GNP+CNT composite. *J. Alloys Compd.* **2022**, *922*, 166110. [[CrossRef](#)]
31. Baskut, S.; Sert, A.; Çelik, O.N.; Turan, S. Anisotropic mechanical and tribological properties of SiAlON matrix composites containing different types of GNPs. *J. Eur. Ceram. Soc.* **2021**, *41*, 1878–1890. [[CrossRef](#)]
32. Zhao, Y.; Yu, T.; Guan, C.; Sun, J.; Tan, X. Microstructure and friction coefficient of ceramic (TiC, TiN and B₄C) reinforced Ni-based coating by laser cladding. *Ceram. Int.* **2019**, *45*, 20824–20836. [[CrossRef](#)]
33. Lu, G.; Shi, X.; Liu, X.; Zhou, H.; Chen, Y. Effects of functionally gradient structure of Ni₃Al metal matrix self-lubrication composites on friction-induced vibration and noise and wear behaviors. *Tribol. Int.* **2019**, *135*, 75–88. [[CrossRef](#)]
34. Cui, G.; Han, B.; Zhao, J.; Li, M. Comparative study on tribological properties of the sulfurizing layers on Fe, Ni and Co based laser cladding coatings. *Tribol. Int.* **2019**, *134*, 36–49. [[CrossRef](#)]
35. Lu, G.; Shi, X.; Liu, X.; Zhou, H.; Chen, Y.; Yang, Z.; Huang, Y. Tribological performance of functionally gradient structure of graphene nanoplatelets reinforced Ni₃Al metal matrix composites prepared by laser melting deposition. *Wear* **2019**, *428–429*, 417–429. [[CrossRef](#)]